



ELSEVIER

Journal of Nuclear Materials 295 (2001) 21–26

Journal of
nuclear
materials

www.elsevier.nl/locate/jnucmat

Ductility and strain rate sensitivity of Zircaloy-4 nuclear fuel claddings

K.W. Lee^a, S.K. Kim^a, K.T. Kim^b, S.I. Hong^{a,*}

^a Department of Metallurgical Engineering, Chungnam National University, Taedok Science Town, Taejeon 305-764, South Korea

^b Research and Development Center, KEPCO Nuclear Fuel Co., Ltd., Taejeon 305-303, South Korea

Received 15 December 2000; accepted 17 February 2001

Abstract

The circumferential mechanical properties of nuclear fuel claddings for Canada deuterium uranium (CANDU) power reactors were examined and the constitutive equation which can predict the temperature dependence of ductility and strain rate sensitivity was developed. The loss of ductility associated with dynamic strain aging was observed between 250°C and 400°C. The elongation minimum results from the concentration of deformation in the necked region in the temperature range of the flow stress plateau. Oxygen atoms actually strengthen the alloy. However, the strengthening of the alloy due to dynamic strain aging decreases the strain rate sensitivity in the temperature range of the flow stress plateau. The decrease in the strain rate sensitivity results in a low ductility. Above the temperature range of the flow stress plateau the elongation of the alloy increases rapidly with temperature. The prediction based on a dynamic strain aging model is in good agreement with the temperature dependence of the circumferential ductility of Zircaloy-4 nuclear fuel claddings. © 2001 Elsevier Science B.V. All rights reserved.

1. Introduction

It is now well established that the strain rate sensitivity of Zircaloy-4 does not increase monotonically with temperature as it is the case for a simple thermally activated process. But the strain rate sensitivity is substantially depressed over a broad temperature range, reaching a minimum over the temperature range where dynamic strain aging occurs [1–8]. In many alloys, the strain rate sensitivity becomes very small in the temperature range of dynamic strain aging [1–8]. Over the whole temperature range, the temperature dependence of elongation follows the same trend as that of strain rate sensitivity [8]. However, the reduction in area at fracture for Zircaloy-4 increases continuously with temperature and there is no minimum in the area reduction [8]. Hong et al. [8] have suggested that oxygen

atoms are responsible for the strain rate sensitivity minimum and the elongation minimum.

The mechanical properties of zirconium and its alloys have been extensively studied in view of their use in nuclear fuel claddings. In most cases, annealed Zr alloy plates and rods have been used to investigate the mechanical properties of Zr alloys. In reality, stress relieved Zr tubes which have a different microstructure and texture from those of annealed plates and rods are used for nuclear fuel claddings. Cladding deformation plays a key role in fuel pellet–clad interaction, with concomitant implications for fuel rod lives. An understanding of the clad deformation behavior is critical to ensure the safe and reliable operation of nuclear power plants. The stress imposed on the claddings due to pellet–clad interaction is mostly hoop stress on the circumference of the tubes and, therefore, the data on the circumferential strength and ductility of nuclear fuel claddings are required. In this paper, the circumferential mechanical properties of nuclear fuel claddings for Canada deuterium uranium (CANDU) power reactors were examined and the constitutive equation which can predict the

* Corresponding author. Tel.: +82-42 821 6587; fax: +82-42 822 9401.

E-mail address: sihong@cnu.ac.kr (S.I. Hong).

Table 1
Chemical composition of Zircaloy-4

Element	Sn	Fe	Cr	O	C	Si	Zr
wt%	1.362	0.214	0.106	0.121	0.013	0.0101	Bal.

temperature dependence of ductility and strain rate sensitivity was developed.

2. Experimental

Commercially produced Zircaloy-4 fuel claddings for CANDU reactors were used in this study. The outer and inner diameters of the claddings were 13.1 and 12.3 mm, respectively, with a wall thickness of 0.4 mm. The composition of the claddings is listed in Table 1. Ring specimens with the width of 5 mm were cut transversely from the cladding tube and tension tested using a special grip. Fig. 1 shows the schematic configuration of the ring specimen and two half-cylinders which open and strain the ring specimen. As shown in this figure, 1 mm wide space was given between two half-cylinders to allow free plastic flow at the beginning of the tensile test. The diameter of the half-cylinders in Fig. 1 was 12.27 mm. Tensile testing was performed using a united testing machine (SFP 10) equipped with a three-zone furnace at room temperature and high temperatures up to 500°C. The close examination of the ring specimens after fracture revealed that no deformation took place in the top and bottom parts of the ring specimen because of the

friction stress between the specimen and the grip (Fig. 1). It is important to estimate the gage length relative accurately since the strain is inhomogeneously distributed along the circumference of the ring specimen. The gage length was determined after a careful comparison between the circumferential (based on the ring tensile test) and longitudinal (based on the split tube tensile test [9]) mechanical properties (yield strength and elongation). Typically, the stress-relieved tubes have the basal poles oriented at about 30° from the tube radial direction, which is close to the radial texture [10–13]. Therefore, the circumferential and longitudinal (both directions are approximately perpendicular to the basal pole) mechanical properties are similar. The gage length in the ring tensile test was determined to be 5 mm by equating the circumferential elongation (from ring tensile testing) to the longitudinal elongation from split tube tensile testing in which the gage length is clearly defined. It was also experimentally confirmed that the

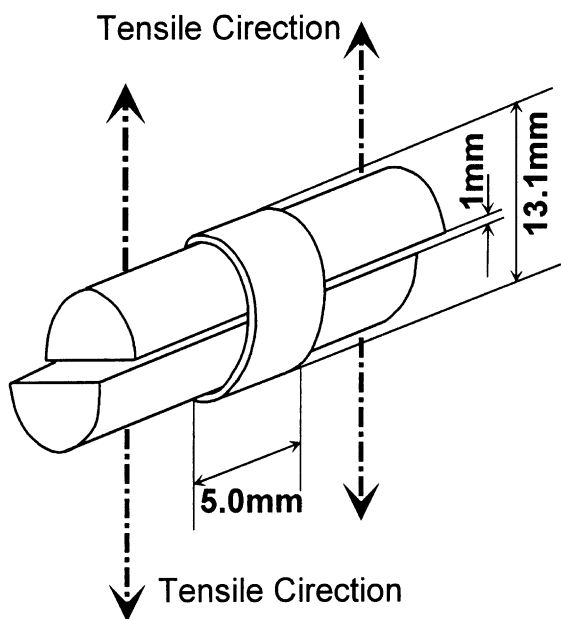


Fig. 1. Schematic configuration of tensile testing sample and grip.

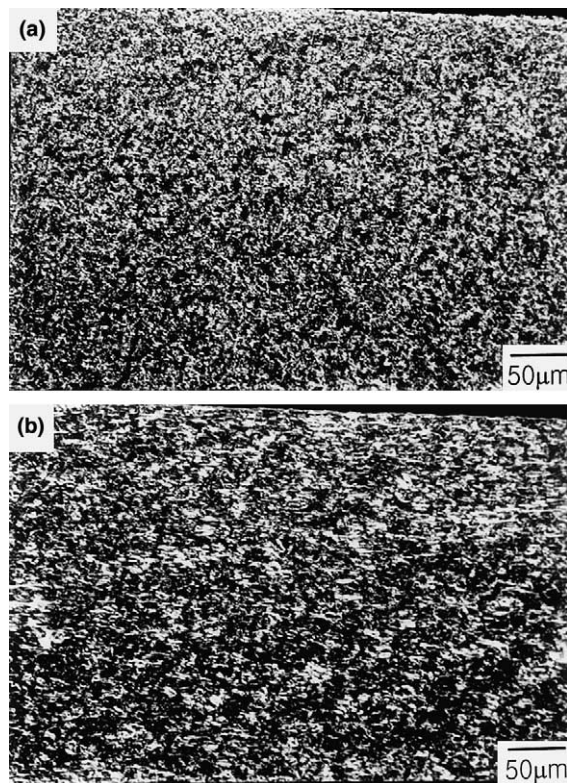


Fig. 2. Transverse (a) and longitudinal (b) microstructures of CANDU nuclear fuel claddings.

deformation occurred only in the left and right-hand side of the specimen within approximately 5 mm width centered on the split line of two half cylinders in Fig. 1. Therefore, the gage length for the calculation of strain rate was assumed to be 5 mm. The fracture surfaces were examined using a JEOL-6400 scanning electron microscope.

3. Results and discussion

Figs. 2(a) and (b) show the very small grains in the transverse (a) and the longitudinal (b) sections of cladding tubes. The grain size in the transverse section was 5.3 μm. The grains are elongated parallel to the tube axis (Fig. 2(b)) in the longitudinal section. Fig. 3 shows the stress–strain responses of Zircaloy-4 CANDU cladding tubes at the strain rate of 1.33 × 10⁻³ s⁻¹ at various temperatures. In the ring tensile testing, the bi-axial stress may develop at the very beginning of the test. However, the space between two split cylinders increases with straining and the stress state may become close to the uni-axial loading, which is supported by the presence of pronounced necking in the fractured specimens. As shown in this figure, there was negligible work hardening and subsequent work softening up to 500°C. The total strain to failure was reduced between 300°C and 400°C. The decrease of the total strain to failure was also observed previously in annealed Zircaloy-4 [8]. Fig. 4(a) shows the circumferential yield strength of Zircaloy-4 cladding tubes as a function of temperature. The plateau of the yield stress is visible over the temperature range between 230°C and 380°C in Fig. 4(a). In Fig. 4(b), the circumferential fracture elongation of the Zircaloy-4 cladding tubes is plotted as a function of temperature. The ductility minimum occurred at each

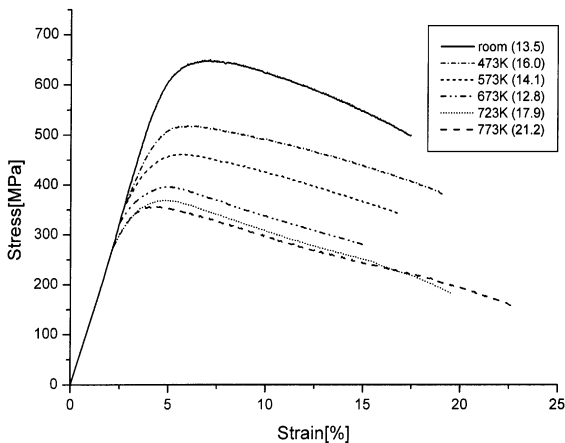


Fig. 3. Stress–strain curve of Zircaloy-4 nuclear fuel claddings at various temperatures.

strain rates and the minimum shifted to higher temperature with increasing strain rate. Fig. 5 shows the fracture surfaces of Zircaloy-4 nuclear fuel claddings. The type of fracture in the temperature region of the elongation minimum is typically of a ductile nature as manifested by the presence of dimples (Figs. 5(c) and (d)).

In the region of dynamic strain aging the total flow stress σ_t is the sum of the stress increment due to dynamic strain aging σ_D and the flow stress σ^* expected in the absence of dynamic strain aging [3,14]:

$$\sigma_t = \sigma^* + \sigma_D. \tag{1}$$

The stress increment σ_D due to dynamic strain aging has its maximum potency at some intermediate temperature and has the form of a statistical normal distribution about temperature [7,8,14,15]:

$$\sigma_D = \sigma_D^0 \exp \left\{ - \frac{(T - \bar{T})^2}{B} \right\}, \tag{2}$$

where σ_D^0 is the maximum value of σ_D , \bar{T} is the temperature at which this maximum occurs and B measures the width of the distribution [16]. For Zircaloy-4 CANDU nuclear fuel claddings, σ_D^0 and B were determined to be

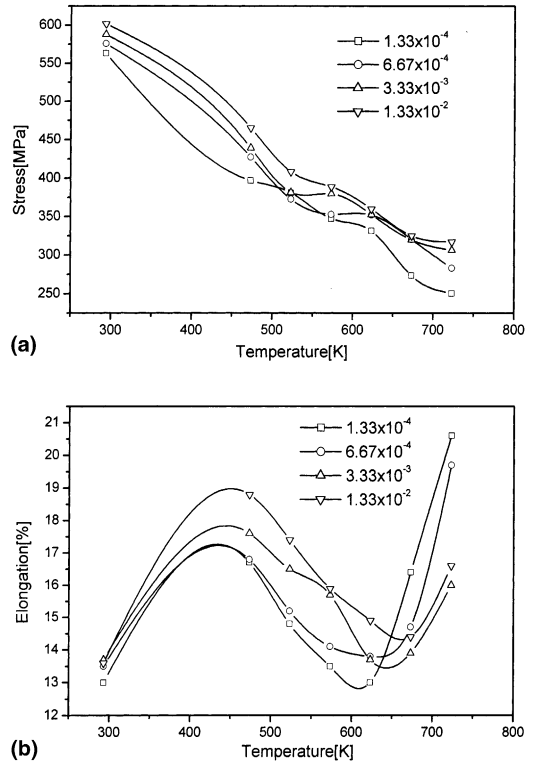


Fig. 4. Variations of yield stress (a) and elongation (b) of CANDU nuclear fuel claddings as a function of temperature and strain rate.

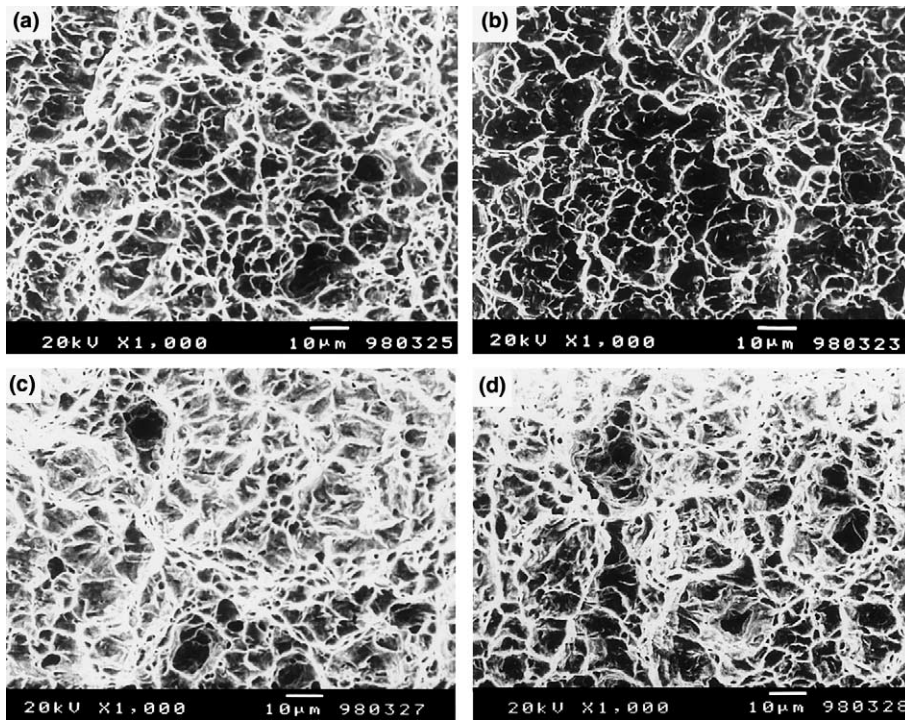


Fig. 5. Fracture surfaces of CANDU nuclear fuel claddings after tensile tests at (a) room temperature, (b) 200°C, (c) 300°C, (d) 400°C.

95.5 MPa and $1.09 \times 10^4 \text{ K}^2$, respectively. The reason for using this equation has been given elsewhere [15–17]. The stress increment σ_D due to dynamic strain aging is strain rate and temperature dependent. When the strain rate rises, σ_D moves towards high temperatures, the plateau leading to a region of low strain rate sensitivity moves towards higher temperatures and accordingly the elongation minimum temperature also increases [8,18]. Hong et al. [8] and Hong [15,18] found that the activation energy obtained from a shift of the elongation minimum temperature with strain rate is equal to that for solute diffusion which is responsible for dynamic strain aging. Hong et al. [8] also suggested that the stress plateau leading to a low strain rate sensitivity and ductility minimum is closely associated with the dynamic interaction between dislocations and oxygen atoms. The shift of the temperature \bar{T} at which the solutes exert the maximum drag force and the elongation minimum occurs can be predicted by the Arrhenius-type equation as follows [8,15,18]:

$$\frac{1}{\bar{T}} = \frac{R}{Q} \ln A - \frac{R}{Q} \ln \dot{\epsilon}, \quad (3)$$

where $\dot{\epsilon}$ is the strain rate (s^{-1}), Q ($= 205 \text{ kJ mol}^{-1}$) [8] is the activation energy for oxygen diffusion in Zircaloy-4, A ($= 9.84 \times 10^{11}$) is a dimensionless constant, and R and T have their usual significance.

The strain rate sensitivity can be calculated from the following usual formula:

$$m_t = \frac{d(\ln \sigma)}{d(\ln \dot{\epsilon})}. \quad (4)$$

Eq. (1) is substituted into Eq. (4) to give

$$m_t = \frac{d\{\ln(\sigma^* + \sigma_D)\}}{d(\ln \dot{\epsilon})} = \frac{1}{\sigma^* + \sigma_D} \left\{ \sigma^* \frac{d(\ln \sigma^*)}{d(\ln \dot{\epsilon})} + \sigma_D \frac{d(\ln \sigma_D)}{d(\ln \dot{\epsilon})} \right\} = \frac{1}{\sigma^* + \sigma_D} (\sigma^* m^* + \sigma_D m_D), \quad (5)$$

where m_t is the observed strain rate sensitivity in alloys, m^* is the strain rate sensitivity expected in the absence of dynamic strain aging as in pure metals and m_D is the contribution of dynamic strain aging to the strain rate sensitivity. Eq. (5) has the same form as that of the creep stress exponent for alloys [19].

The strain rate sensitivity m^* in the absence of dynamic strain aging tends to rise linearly with increasing absolute temperature [3,20]. Therefore, m^* can be expressed as

$$m^* = \frac{d(\ln \sigma^*)}{d(\ln \dot{\epsilon})} = \alpha T + \beta, \quad (6)$$

where α and β are constants. From Eq. (6) we can obtain the following equation:

$$\sigma^* = \sigma_D^* \left(\frac{\dot{\epsilon}}{\dot{\epsilon}_0} \right)^{\alpha T + \beta}, \quad (7)$$

where σ_D^* and $\dot{\epsilon}_0$ are constants. The contribution of dynamic strain aging to the strain rate sensitivity can be calculated from the following equation:

$$m_D = \frac{d(\ln \sigma_D)}{d(\ln \dot{\epsilon})} = \frac{d(\ln \sigma_D)}{dT} \frac{dT}{d(\ln \dot{\epsilon})} = \frac{2R(T - \bar{T})\bar{T}^2}{BQ}. \quad (8)$$

Now we can calculate the strain rate sensitivity from Eq. (5). For a good fit between the data of this study and the strain rate sensitivity predicted from Eq. (5), $\alpha, \beta, \sigma_D^*$ and $\dot{\epsilon}_0$ determined to be $2.04 \times 10^{-4} \text{ K}^{-1}$, -5.3×10^{-2} , 636 MPa and $1.498 \times 10^3 \text{ s}^{-1}$, respectively. The line predicted by Eq. (5) is in reasonably good agreement with the experimental data, as shown in Fig. 6. The strain rate sensitivity minimum occurs at each strain rate and the minimum is shifted to higher temperature with increasing strain rate.

It is well-known that the elongation is a sensitive function of the strain rate sensitivity [14,20–23]. It can be assumed that the fracture strain is a linear function of the strain rate sensitivity for some alloys:

$$\epsilon_f(\%) = a m_t + b, \quad (9)$$

where a and b are constants. If the strain rate sensitivity is high, the increase in strain rate in the necked region may increase the resistance to flow sufficiently so that deformation tends to occur above and below the neck, resulting in a high ductility. However, the low strain rate sensitivity concentrates the deformation in the neck, once a neck is formed, resulting in a low ductility. For a good fit of the fracture strain predicted by Eqs. (5) and

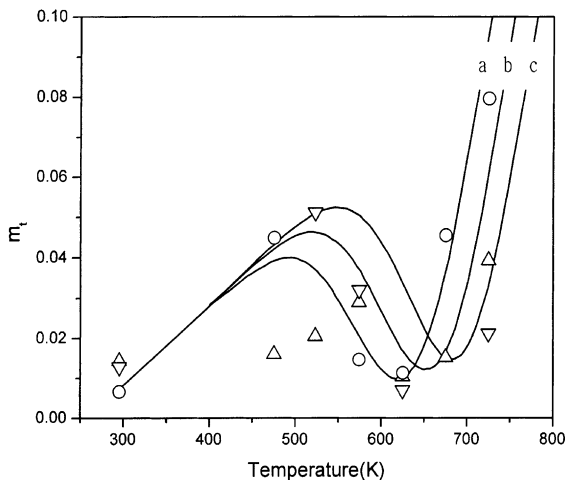


Fig. 6. Temperature dependence of the predicted (curves a)–(c) and measured (\circ , \triangle , ∇) strain rate sensitivity of flow stress for the three strain rates, $1.33 \times 10^{-4} \text{ s}^{-1}$ (curve a, \circ), $6.67 \times 10^{-4} \text{ s}^{-1}$ (curve b, \triangle) and $3.33 \times 10^{-3} \text{ s}^{-1}$ (curve c, ∇).

(9) to the data of the present study, a and b were determined to be 100 and 12.9, respectively. As shown in Fig. 7, the predicted line is in reasonably good agreement with the experimental data.

As stated previously, there is no minimum in the area reduction in Zircaloy-4 (see [8], Fig. 2). This result implies that the elongation minimum is apparently not associated with brittle fracture. In Zr alloys the low ductility is associated with the low strain rate sensitivity due to dynamic strain aging. To distinguish the low ductility which is due to grain boundary segregation of solutes as observed in steels [24–26], the phenomenon associated with the low ductility due to low strain rate sensitivity was termed ‘indirect solute embrittlement’, and the low ductility due to the grain boundary segregation of solute atoms was termed ‘direct solute embrittlement’ [14]. The reason for the term ‘indirect solute embrittlement’ is that solute atoms do not cause the low ductility directly but actually strengthen the alloy. However, the strengthening of the alloy due to dynamic strain aging reduces the strain rate sensitivity [8]. In many alloys, both mechanisms may contribute to the low ductility at the same time. The main difference between them may be the role of solute atoms at grain boundaries [8]. Solute atoms apparently weaken the grain boundaries in direct solute embrittlement but do not do so in the indirect solute embrittlement. The type of fracture in indirect solute embrittlement is typically of a ductile nature whereas the fracture in direct solute embrittlement involves low energy fracture along grain boundaries.

The temperature region in which the elongation minimum occurs corresponds to the plateau in the flow stress vs. temperature curve [8]. This model also predicts a rapid increase in elongation above the temperature

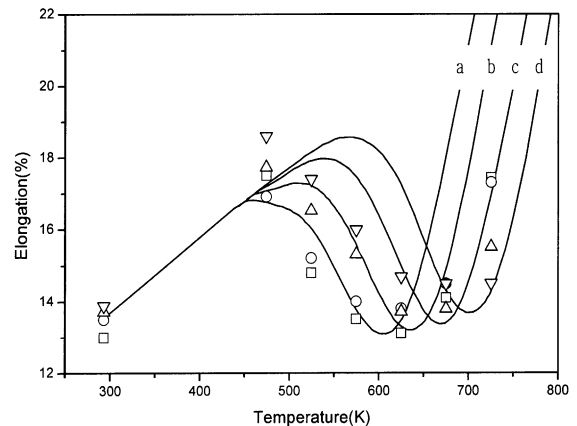


Fig. 7. Predicted (curves a)–(d) and measured (\square , \circ , \triangle , ∇) percentage elongation of CANDU(13.1) claddings vs. temperature for the four strain rates, $1.33 \times 10^{-4} \text{ s}^{-1}$ (curve a, \square), $6.67 \times 10^{-4} \text{ s}^{-1}$ (curve b, \circ), $3.33 \times 10^{-3} \text{ s}^{-1}$ (curve c, \triangle), $1.33 \times 10^{-2} \text{ s}^{-1}$ (curve d, ∇).

range of the flow stress plateau where the flow stress rapidly decreases. Experimental data show a significant increase in ductility above the elongation minimum temperature, which is in good agreement with this prediction [8]. As suggested by Hong [14], the macroscopic deformation mode can be related to the microscopic dislocation structure. In the temperature region of the flow stress plateau, dynamic strain aging causes microscopically the clustering of dislocations [18] and macroscopically the concentration of deformation in the neck. Above the temperature range of the plateau, dynamic strain aging causes microscopically the homogeneous distribution of dislocations [18] and macroscopically the spread-out of deformation over the entire gauge section.

4. Conclusions

In this study a constitutive equation is derived which can predict the temperature dependence of elongation for Zircaloy-4 CANDU nuclear fuel claddings. The loss of ductility associated with dynamic strain aging was observed between 250°C and 400°C. The elongation minimum results from the concentration of deformation in the necked region in the temperature range of the flow stress plateau. Oxygen atoms actually strengthen the alloy. However, the strengthening of the alloy due to dynamic strain aging decreases the strain rate sensitivity in the temperature range of the flow stress plateau. The decrease in the strain rate sensitivity results in a low ductility. Above the temperature range of the flow stress plateau the elongation of the alloy increases rapidly with temperature. The prediction based on a dynamic strain aging model is in good agreement with the temperature dependence of the circumferential ductility of Zircaloy-4 nuclear fuel claddings.

References

- [1] S.N. Tiwari, D.J. Lloyd, K. Tangri, *Metall. Trans.* 3 (1972) 2605.
- [2] M.J. Luton, J.J. Jonas, *Can. Metall. Q.* 11 (1972) 79.
- [3] J.D. Lubahn, *Trans. Metall. Soc. AIME* 185 (1949) 702.
- [4] D. Lee, *Metall. Trans.* 1 (1970) 1607.
- [5] V. Ramachandran, R.E. Reed-Hill, *Metall. Trans.* 1 (1970) 2105.
- [6] A.M. Garde, E. Aigeltinger, B.N. Woodruff, R.E. Reed-Hill, *Metall. Trans.* (1975) 1183.
- [7] A.K. Miller, O.D. Sherby, *Acta Metall.* 26 (1978) 289.
- [8] S.I. Hong, W.S. Ryu, C.S. Rim, *J. Nucl. Mater.* 116 (1983) 314.
- [9] D.D. Himbeault, C.K. Chow, M.P. Puls, *Metall. Trans.* 25A (1994) 135.
- [10] K.P. Steward, B.A. Cheadle, *Trans. Metall. Soc. AIME* 239 (1967) 504.
- [11] B.A. Cheadle, in: W. Evans, J.A.L. Robertson (Eds.), *The Physical Metallurgy of Zirconium Alloys*, CRNL-1208, 1974, p. 51.
- [12] B.A. Cheadle, C.E. Ells, W. Evans, *J. Nucl. Mater.* 23 (1967) 199.
- [13] J.C. Wood, *J. Nucl. Mater.* 45 (1972/73) 105.
- [14] S.I. Hong, *Mater. Sci. Eng.* 91 (1987) 137.
- [15] S.I. Hong, *Mater. Sci. Eng.* 76 (1985) 77.
- [16] S.I. Hong, W.S. Ryu, C.S. Rim, *J. Nucl. Mater.* 120 (1984) 1.
- [17] S.I. Hong, *Mater. Sci. Eng.* 86 (1987) 211.
- [18] S.I. Hong, *Mater. Sci. Eng.* 79 (1986) 1.
- [19] S.I. Hong, *Mater. Sci. Eng.* 82 (1986) 175.
- [20] R.E. Reed-Hill, in: *Physical Metallurgy Principles*, Van Nostrand, New York, 1973, p. 348.
- [21] R.W. Lund, W.D. Nix, *Acta Metall.* 24 (1975) 469.
- [22] F.A. Mohamed, *Scr. Metall.* 12 (1978) 99.
- [23] M.A. Burke, W.D. Nix, *Acta Metall.* 23 (1975) 793.
- [24] H. Ohtani, C.J. McMahon Jr., *Acta Metall.* 23 (1975) 319.
- [25] M.L. Jokl, V. Vitke, C.J. McMahon Jr., *Acta Metall.* 23 (1975) 377.
- [26] C.J. McMahon Jr., *Mater. Sci. Eng.* 42 (1980) 215.